Ferroelectric domain structure in epitaxial $BiFeO_3$ films

F. Zavaliche
Materials Research Science and Engineering Center, University of Maryland, College Park, Maryland 20742

R. R. Das, D. M. Kim, and C. B. Eom
Department of Materials Science and Engineering, University of Wisconsin, Madison, Wisconsin 53706

S. Y. Yang, P. Shafer, and R. Ramesh
Department of Materials Science and Engineering, and Department of Physics, University of California, Berkeley, California 94720

(Received 14 March 2005; accepted 13 September 2005; published online 28 October 2005)

Piezoelectric force microscopy is employed to study the ferroelectric domain structure in a 600 nm thick epitaxial $BiFeO_3$ film. In the as-grown film, a mosaic-like domain structure is observed. Scans taken with the cantilever pointing along the principal crystallographic directions enabled us to reconstruct the polarization direction. By combining the perpendicular and in-plane piezoresponse data, we found that the ferroelectric domain structure is mainly described by four polarization directions. These directions point oppositely along two body diagonals, which form an angle of ~71°. The other variants are also occasionally observed. © *2005 American Institute of Physics*. [DOI: 10.1063/1.2126804]

A renewed interest in $BiFeO_3$ has been stimulated by the coexistence of ferroelectricity[1] and weak ferromagnetism at ambient conditions, observed in both a single phase[2] and in solid solutions.[3] $BiFeO_3$ is characterized by a rhombohedrally distorted perovskite structure having unit cell parameters a_r=3.96 Å and α_r=0.6°;[4,5] bulk ceramics showed small values of polarization. In contrast, epitaxial thin films have exhibited large polarization with structures sensitive to the heteroepitaxial constraints.[2,6] The high polarization and piezoelectric response in thin $BiFeO_3$ films suggests a possible environmentally benign substitute for Pb-based ferroelectrics, though considerable optimization of ferroelectric properties is necessary.[7] This requires a comprehensive understanding of the equilibrium domain structure as well as the effects of dopants (e.g., La in the Bi site). In this letter, we present results of piezoresponse force microscopy (PFM)[8–10] experiments aimed at understanding the equilibrium domain configuration in epitaxial $BiFeO_3$ films.

A 600 nm thick film was grown by magnetron sputtering on $SrTiO_3$(001) with a thin epitaxial $SrRuO_3$ bottom electrode.[11] The details of growth, structural, and electrical properties of the $BiFeO_3$ films are reported elsewhere.[12] The films grew in the rhombohedral state, since the ferroelectric Curie temperature is ~800 °C. This was confirmed by x-ray diffraction.[12] The ferroelectric domain structure was studied at ambient conditions by PFM, using an ac bias of 3.0 V_{pp} at 6.39 kHz applied to the conducting probe. Out-of-plane (OP) and in-plane (IP) piezoelectric response (PR) signals were simultaneously recorded to reconstruct the direction of polarization. Amplitude (R) and phase (θ) information are included in each image, since the in-phase PR signals ($X=R\cos\theta$) were acquired to image the domains. Our experimental results are discussed within the frame of the crystallographic model of Kubel and Schmid.[4] Thus, on a (001) surface, four structural variants (eight polarization variants) schematically represented in Fig. 1 can fully describe the ferroelectric domain structure.

A mosaic-like ferroelectric domain structure was observed in both OP and IP-PFM images (Figs. 2 and 3). We establish the convention that light and dark IP tones stand for right and left polarization components, respectively, with respect to the cantilever's long axis. By locally poling the film at negative and positive biases above the threshold value we found that the dark and light regions in the OP-PFM images are domains with up and down OP polarization components, respectively. An additional weak contrast can be distinguished in the OP-PFM images, which matches the IP-PFM domain pattern. This weak contrast accounts for about 15% of the signal measured between the up and down polarization states. This can be understood as a possible consequence of a mechanical effect, which arises from the different relative orientations of the polarization vector with respect to both

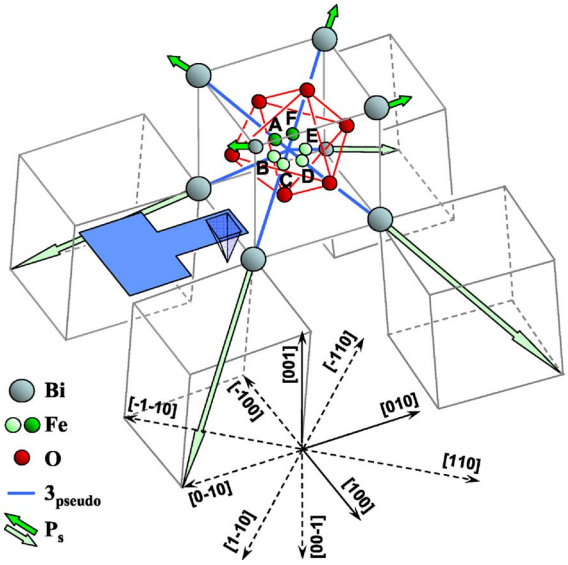

FIG. 1. (Color online) A sketch of perovskite building blocks in the rhombohedral structure. Shown in the central unit are possible Fe positions in the ferroelectric state (A–F). Polarization directions are marked with arrows.

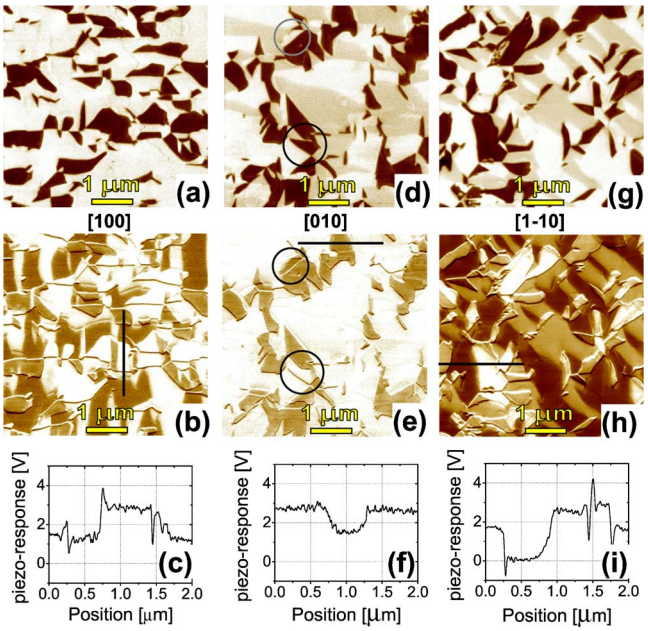

FIG. 2. (Color online) (a), (d), (g) OP and (b), (e), (h) IP-PFM images taken with the cantilever pointing along the directions marked on the figure. (c), (f), (i) IP-PR signal measured along the lines in the corresponding PFM images. Spikes in the plots are due to domain walls.

the cantilever's long axis and clamping point. The sketch in Fig. 1 illustrates such a configuration with the cantilever pointing along [010].

The scans in Fig. 3 were acquired with the cantilever pointing along the same axes as in Fig. 2, but in opposite directions. The reason for doing this is to independently confirm the ⟨111⟩ polarization vector directions. Due to the complicated domain pattern observed in the PFM scans, we could not *a priori* assume that the interpretations based on scans along just one direction are accurate. To do so, the sample was rotated and due to the geometrical constraints of

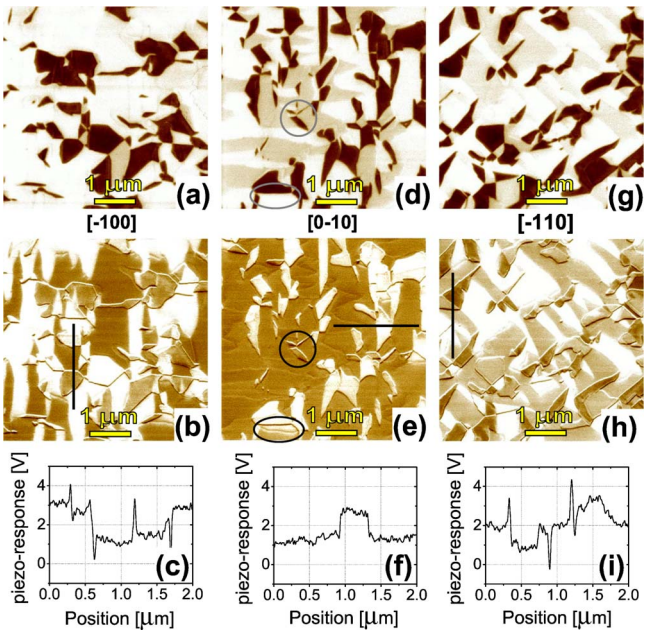

FIG. 3. (Color online) (a), (d), (g) OP and (b), (e), (h) IP-PFM images taken with the cantilever pointing along the directions marked on the figure. (c), (f), (i) IP-PR signal measured along the lines in the corresponding PFM images.

TABLE I. The possible polarization orientations deduced from the OP and IP images in Figs. 2(d), 2(e), 3(d), and 3(e).

OP contrast	IP contrast		Possible orientations
	[010]	[0-10]	
Dark (up)	Dark (left)	Light (right)	[-111], [-1-11]
Light (down)	Light (right)	Dark (left)	[1-1-1], [11-1]

the microscope, the images could no longer be recorded in exactly the same area. The IP projection of the ⟨111⟩ polarization vectors on a (001) surface lie along the pseudocubic ⟨110⟩ axes.[13] Thus, PFM scans taken with the cantilever pointing in opposite directions along one of the ⟨110⟩ axes provide the same contrast levels for the IP-polarization components as scans taken with the cantilever along the other ⟨110⟩ axis. Indeed, this was confirmed in our scans, and therefore only one set of data is shown in Figs. 2(g), 2(h), 3(g), and 3(h). This IP information, corroborated with the two possible OP orientations enable a complete 3D description of polarization orientation, as shown earlier.[14–16]

The IP-PFM images taken with the cantilever pointing along the ⟨100⟩ axes [Figs. 2(b), 2(e), 3(b), and 3(e)] exhibit two contrast levels, while scans performed with the cantilever pointing along ⟨110⟩ show three levels [Figs. 2(h) and 3(h)]. Line profiles across the images in Figs. 2(b) and 3(b) reveal PR signal magnitudes of ~2.9 and ~1.2 V in both images. For scans taken with the cantilever pointing along the other ⟨100⟩ axis [Figs. 2(e) and 3(e)], the two levels correspond to ~2.7 and ~1.3–1.5 V [Figs. 2(f) and 3(f)]. Since only two levels are observed in these IP-PFM images and the corresponding PR signals are the same for scans performed with the cantilever pointing oppositely along the same axis, the IP-polarization components symmetrically straddle each of the ⟨100⟩ axes. Thus, we make the inference that these components can only lie along ⟨110⟩, in agreement with the Kubel and Schmid's model.[4] This is confirmed by the IP-PFM scans taken with the cantilever pointing along the ⟨110⟩ axes [Figs. 2(h) and 3(h)]. In these images, the PR signal corresponding to the light-hued tone (~1.7 V in Fig. 2(i) and ~2.0 V in Fig. 3(i)), changes only slightly as the sample is rotated by 180°. Therefore, the IP polarization components of these domains lie along the cantilever's axis. Rotating the sample by 180° [Figs. 3(g) and 3(h)] inverts the IP-PR almost symmetrically about the neutral level (light-hued domains). The neutral level is also observed in the IP-PFM images taken with the cantilever along the other two orthogonal ⟨110⟩ axes (not shown), confirming the ⟨111⟩ orientation of polarization.

In the images taken with the cantilever pointing along [010] [Figs. 2(d) and 2(e)] and [0$\bar{1}$0] [Figs. 3(d) and 3(e)], most of the domains with up-polarization are predominantly one tone in the IP-PFM images, while domains with down-polarization exhibit the opposite IP contrast. The possible orientations of polarization resulting from these findings are summarized in Table I. Thus, the domain structure is mainly characterized by four polarization vectors oriented oppositely along two body diagonals, which form an angle of 71° with each other. A minute amount of the other four variants [circled in Figs. 2(d), 2(e), 3(d), and 3(e)] is also seen.

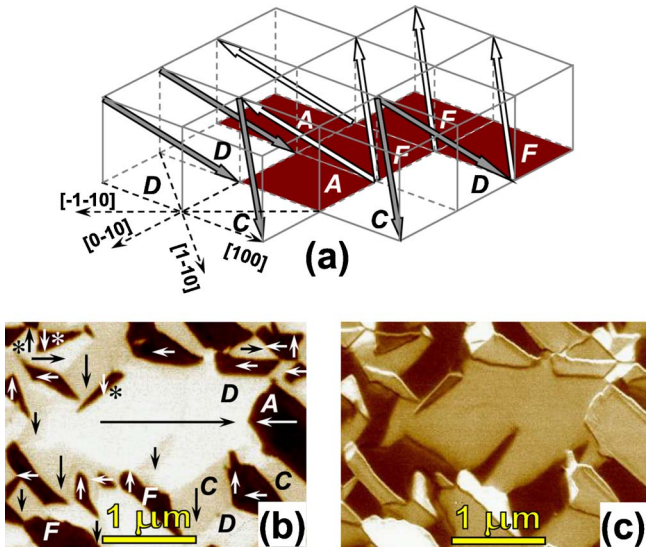

FIG. 4. (Color online) (a) A three-dimensional sketch of the main polarization directions. (b) OP and (c) corresponding IP-PFM images taken along $[\bar{1}\bar{1}0]$. The arrows in (b) represent the directions of IP polarization components, as deduced from (c). Some of the domains in (b) are marked with the same letters as the ones used in Fig. 1.

The main polarization directions in the mosaic domain structure are schematically shown in Fig. 4(a) and are identified in the OP-PFM scan in Fig. 4(b), taken with the cantilever pointing along $[\bar{1}\bar{1}0]$. Shown in Fig. 4(c) is the corresponding IP-PFM image. The domains were labeled according to the different Fe cation sites in Fig. 1, namely A and F for up-polarization domains, and C, D for down-polarization domains, as deduced from the levels in Fig. 4(c). Note that there is a small degree of uncertainty for IP-polarization components along the scanning direction due to the occasional occurrence of the other two variants. These variants are identified among the domains with IP polarization components perpendicular to the cantilever's long axis, and are marked with an asterisk in Fig. 4(b). Both ferroelectric (A–D, F–C) and ferroelastic (A–C, A–F, F–D, C–D) domain walls can be distinguished. The consideration of IP components only in Fig. 4(b) can be misleading, since head-to-head domains apparently occur. In fact, by taking into account the OP components, one finds that this is an allowed configuration that leads to the formation of ferroelectric domain walls.

In summary, based on PFM data, we have investigated the ferroelectric domain structure in a 600 nm thick epitaxial $BiFeO_3$ film. The mosaic domain configuration in the as-grown film is mainly described by four polarization directions orientated oppositely along two body diagonals that form an angle of $\sim 71°$. This domain configuration leads to the formation of both ferroelectric and ferroelastic domain walls.

This work has been supported in part by the University of Maryland NSF-MRSEC under Grant No. DMR 00-80008, and by the ONR under a MURI program. The authors acknowledge the support of the NSF-FRG under Awards No. DMR-0313764, No. ECS-0210449, No. DMR-0103354, and a David & Lucile Packard Fellowship (C.B.E.).

[1] J. R. Teague, R. Gerson, and W. J. James, Solid State Commun. **8**, 1073 (1970).
[2] J. Wang, J. B. Neaton, H. Zheng, V. Nagarajan, S. B. Ogale, B. Liu, D. Viehland, V. Vaithyanathan, D. G. Schlom, U. V. Waghmare, N. A. Spaldin, K. M. Rabe, M. Wuttig, and R. Ramesh, Science **299**, 1719 (2003).
[3] K. Ueda, H. Tabata, and T. Kawai, Appl. Phys. Lett. **75**, 555 (1999).
[4] F. Kubel and H. Schmid, Acta Crystallogr., Sect. B: Struct. Sci. **B46**, 698 (1990).
[5] C. Michel, J.-M. Moreau, G. D. Achenbechi, R. Gerson, and W. J. James, Solid State Commun. **7**, 701 (1969).
[6] J. Li, J. Wang, M. Wuttig, R. Ramesh, N. Wang, B. Ruette, A. P. Pyatakov, A. K. Zvezdin, and D. Viehland, Appl. Phys. Lett. **84**, 5261 (2004).
[7] X. Qi, M. Wei, Y. Lin, Q. Jia, D. Zhi, J. Dho, M. G. Blamire, and J. L. MacManus-Driscoll, Appl. Phys. Lett. **86**, 071913 (2005).
[8] P. Güthner and K. Dransfeld, Appl. Phys. Lett. **61**, 1137 (1992).
[9] A. Gruverman, O. Auciello, and H. Tokumoto, Annu. Rev. Mater. Sci. **28**, 101 (1998).
[10] S. V. Kalinin and D. A. Bonnell, Phys. Rev. B **65**, 125408 (2002).
[11] C. B. Eom, R. J. Cava, R. M. Fleming, J. M. Phillips, R. B. van Dover, J. H. Marshall, J. W. P. Hsu, J. J. Krajewski, and W. F. Peck Jr., Science **258**, 1766 (1992).
[12] R. R. Das, D. M. Kim, S. H. Baek, F. Zavaliche, S. Y. Yang, X. Ke, S. K. Streiffer, M. S. Rzchowski, R. Ramesh and C. B. Eom, Appl. Phys. Lett. (submitted).
[13] All Miller indices are based on pseudo cubic lattice and not rhombohedral.
[14] L. M. Eng, H.-J. Güntherodt, G. A. Schneider, U. Köpke, and J. Muñoz Saldaña, Appl. Phys. Lett. **74**, 233 (1999).
[15] M. Abplanalp, D. Barošová, P. Bridenbaugh, J. Erhart, J. Fousek, P. Günter, J. Nosek, and M. šulc, J. Appl. Phys. **91**, 3797 (2002).
[16] C. S. Ganpule, V. Nagarajan, B. K. Hill, A. L. Roytburd, E. D. Williams, R. Ramesh, S. P. Alpay, A. Roelofs, R. Waser, and L. M. Eng, J. Appl. Phys. **91**, 1477 (2002).